Bremsstrahlung from fully stripped tungsten (W^{74+}) in a Debye-Hückel potential

Ju Yan Wu [1], Yongjun Cheng,[1] Andrius Poškus [2], Yong Wu,[3,4] Jian Guo Wang,[3] and Song Bin Zhang [1,*]

[1]*School of Physics and Information Technology, Shaanxi Normal University, Xi'an 710119, China*
[2]*Institute of Chemical Physics, Vilnius University, Saulėtekio al. 9, Building III, Vilnius LT-10222, Lithuania*
[3]*Institute of Applied Physics and Computational Mathematics, P.O. Box 8009, Beijing 100088, China*
[4]*Center for Applied Physics and Technology, Peking University, Beijing 100084, China*

Based on the exact relativistic multipole calculations using pure Coulomb and Debye-Hückel potentials, discussions of bremsstrahlung cross sections and corresponding emitted photon angular distributions from fully stripped tungsten (W^{74+}) are given for electron scattering at energies of 10–150 keV. Nonrelativistic dipole calculations are also presented, showing that for the above energy region, the nonrelativistic results are completely invalid and the relativistic and multipole effects must be taken into account. The reduction of bremsstrahlung cross sections due to screening of the nuclear charge is studied using the relativistic multipole method at different values of the screening length and photon energy. With an increase of electron scattering energy, the effect of the screening potential on both the dynamics of fast free electrons and the cross sections is reduced. The peak of the angular distribution of bremsstrahlung would shift towards smaller emission angles when the screening strength is reduced.

I. INTRODUCTION

As the typical material of the first wall and divertor in tokamaks [1–3], extensive investigations of tungsten (W) and its ions for the plasma interactions are of great interest and importance since damages of the wall material by the runaway electrons (entering into the host environment by sputtering [4–8]) are unavoidable, and the artificial disruptions of radiation damage [9–11] are also usually needed [12–14]. In addition to the electronic structures and radiation spectra of these impurities, the related quantum collision cross sections and radiation rates are also very important for the understanding of energy transfer and plasma wall damages [10,11,15].

In this work, we present first-hand relativistic investigations of the bremsstrahlung process of tungsten ions, taking into account the plasma screening effects. Such a radiation process is also an important way of energy transport in the astrophysical systems, magnetic confinement fusion (MCF), inertial confinement fusion (ICF), laser material interaction, and so on [16–18]. In a high-temperature environment, bremsstrahlung is the dominant mechanism involved in plasma-wall interactions [19,20]. The radiation process strongly depends on the temperature and density of plasmas. The proper experimental designs could reduce the highly charged impurities and the corresponding high photon damages from bremsstrahlung, asking for comprehensive theoretical investigations of this process of the impurities [21–23].

Bremsstrahlung is a typical free-free radiation process, calculations of cross sections require the evaluations of overlap matrix elements (for the multipole expansion of radiation field [24]) between the (initial and final relativistic) continuum wave functions, causing great difficulties to achieve converged results [25]. In the 1930s, Bethe and Heitler proposed a general semi-classical formula based on Born approximation for the relativistic bremsstrahlung [26], which is known as the BH formula and has been broadly used and improved by many works for a long time [27,28]; in the high scattering energy region, the modified BHE formula [27] could provide reasonable results in a very cheap way.

In the 1970s, Tseng and Pratt proposed the relativistic first-principle method to calculate accurate bremsstrahlung emission cross sections [29,30] by partial-wave expansion [24], which laid the foundations of extensive research on ordinary bremsstrahlung. Note that in double partial-wave expansions (for both the initial and final electronic wave functions), the total number of matrix terms increases exponentially with energy to obtain reliable cross sections [30]. Many investigations have been performed [31–34] and related program packages have been developed [35–37] for limited energies from a few eV to tens of MeV.

However, as far as we know, studies of the bremsstrahlung process with tungsten ions are still absent, especially considering the screening effects of plasmas, and such a plasmas environment has been shown to be important in other dynamic processes [25,38–48]. One possible reason is that, with the increase of atomic number, the relativistic and multipole effects are enhanced, requirements on the theoretical side are stricter, and the required mathematical processing is more complicated. To distinguish the relativistic and multipole effects from the nonrelativistic dipole calculations [25,49,50] and show its different physical variations in plasmas environments, the relativistic multipole bremsstrahlung process of W^{74+} is

*song-bin.zhang@snnu.edu.cn

studied in the present work, with the help of the code BREMS recently released by one of the coauthors [51]. Explicitly, the cross sections and angular distributions of relativistic multipole bremsstrahlung are given in a large energy region in both the pure Coulomb potential and Debye-Hückel screened potential, and the related physical properties are discussed.

The organization of this article is as follows. The relevant theories of bremsstrahlung in relativistic multipole theory are described briefly in Sec. II. In Sec. III, the numerical results of bremsstrahlung cross sections and its angular distributions are given and discussed and the results are compared with those in nonrelativistic dipole theory. Concluding remarks are given in Sec. IV. Relativistic units ($\hbar = m_e = c = 1$) are used throughout this paper. Note that in relativistic units, one unit of length equals the reduced Compton wavelength of the electron $\lambda_e = \hbar/m_e c = 3.861592 \times 10^{-11}$ cm $= 386.1592$ fm, one unit of time is the interval in which light travels one reduced Compton wavelength of the electron $\hbar/m_e c^2 = 1.288088 \times 10^{-21}$ s, and the electron rest energy $m_e c^2 = 0.5110041$ MeV equals to one unit of energy [52,53].

II. COMPUTATIONAL METHODS

For the photon emissions, there are ordinary bremsstrahlung and polarization bremsstrahlung [31,54,55], we study the first one in the relativistic framework. The nonrelativistic calculation is also performed for comparison using the methods reported in [56]. Tseng and Pratt [24] presented a detailed relativistic treatment of bremsstrahlung in which the multipole effect is also included; here we only introduce the formulas needed in the present work.

Let θ and Ω_k be the angles of the emitted photon momentum $\vec{k}$ with respect to the incident electron momentum $\vec{p}_1$ and the element of the solid angle in the direction of $\vec{k}$, respectively, the scaled bremsstrahlung differential cross section $\sigma(k, \theta)$ with respect to the photon energy and emission angle is given by [24]

$$
\begin{aligned}
\sigma(k, \theta) &= \frac{\beta_1^2 k}{Z^2} \frac{d\sigma}{dk d\Omega_k} \\
&= \lambda_0 \beta_1^2 \sum_{\kappa_1 \bar{\kappa}_1 \kappa_2} (-1)^{l_1 + \bar{l}_1} \cos\left(\delta_{\kappa_1} - \delta_{\bar{\kappa}_1}\right) \\
&\quad \times \sum_{m \equiv |m_2|} [A_+^+(m)\bar{A}_+^+(m) + A_+^-(m)\bar{A}_+^-(m) \\
&\quad\quad + A_-^+(m)\bar{A}_-^+(m) + A_-^-(m)\bar{A}_-^-(m)]. \quad (1)
\end{aligned}
$$

Here the set of values of $\bar{l}_1$ and $\bar{\kappa}_1$ is the same as that of l_1 and κ_1 and they are used to represent a different summation. The bar over $A_\pm^\pm$ corresponds to the replacement of κ_1 and l_1 with $\bar{\kappa}_1$ and $\bar{l}_1$ in the calculation.

Then the scaled bremsstrahlung cross section $\sigma(k)$, or the photon energy differential cross section, can be obtained by integrating $\sigma(k, \theta)$ over $d\Omega_k$ written as [24]

$$
\frac{\beta_1^2 k}{Z^2} \frac{d\sigma}{dk} \equiv \sigma(k) = \lambda_0 \beta_1^2 \sum_{\kappa_2, \kappa_1, m = |m_2|} \left\{ \left[R_{\kappa_2 \kappa_1}^+(m)\right]^2 \right.
$$
$$
\left. + \left[R_{\kappa_2 \kappa_1}^-(m)\right]^2 \right\}. \quad (2)
$$

The factor $\beta_1^2(k/Z^2)$ is used to eliminate the known dependence on these factors, resulting in a reduced variation of $\sigma(k)$ [57], and Z is the nuclear charge. Note that the initial electron is unpolarized, and the cross section obtained in Eq. (2) is the single differential cross section (SDCS), although it is called the total cross section in the present work. Similarly the cross section in Eq. (1) is actually the double differential cross section (DDCS).

In Eqs. (1) and (2), the parameter $\beta_1 = \frac{v_1}{c} = \frac{\sqrt{T_1(T_1+2)}}{T_1+1}$ is the ratio of the initial electron speed v_1 to the speed of light c and T_1 is the kinetic energy of the incident electron. $\lambda_0 = (3.86144)^2 \times 10^5 \times \frac{32\alpha}{Z^2 p_1} E_1 E_2 p_2 k^2$, where p_1 (p_2) and E_1 (E_2) are the momentum and total energy of initial (final) electrons, respectively. δ_k is the phase shift;

$$
\begin{aligned}
A_\pm^+(m) &= C_{\kappa_1, m-1}^\pm y_{l_1, m-1 \mp \frac{1}{2}}(\theta) R_{\kappa_2 \kappa_1}^+(m), \\
A_\pm^-(m) &= C_{\kappa_1, m+1}^\pm y_{l_1, m+1 \mp \frac{1}{2}}(\theta) R_{\kappa_2 \kappa_1}^-(m), \quad (3)
\end{aligned}
$$

where $C_{\kappa, m}^\pm = C(l \frac{1}{2} j; m \mp \frac{1}{2}, \pm \frac{1}{2})$ is the Clebsch-Gordan coefficient, $y_{lm}(\theta)$ is the pre-exponential factor of the spherical harmonic $Y_{lm}(\theta, \phi) = y_{lm}(\theta) e^{im\phi}$ with azimuth angle ϕ, and

$$
R_{\kappa_2 \kappa_1}^\pm(m) = \sum_{n=1}^{2} Q_n^\pm(m) \sum_l P_n^\pm(m) S_n. \quad (4)
$$

Symbols κ (κ_1 or κ_2) represent the partial-wave quantum numbers of the initial or final states, which are defined by the orbital angular momentum l and the total angular momentum j, namely $\kappa = l$ for $j = l - \frac{1}{2}$ and $\kappa = -l - 1$ for $j = l + \frac{1}{2}$. m (m_1 or m_2) is the magnetic quantum number corresponding to κ (κ_1 or κ_2). The index l takes value from $|l_2' - l_1|$ to $l_2' + l_1$ in steps of 2 for $n = 1$, and from $|l_2 - l_1'|$ to $l_2 + l_1'$ in steps of 2 for $n = 2$. In addition, other parameters are $l' = l + \eta_\kappa$ and $\eta_\kappa = -\kappa/|\kappa|$. Q_n and P_n are related to the angular couplings [24], and S_n is the overlapping integral of continuum wave functions, defined as

$$
\begin{aligned}
S_1 &= \int_0^\infty j_l(kr) g_{\kappa_1}(r) f_{\kappa_2}(r) dr, \\
S_2 &= \int_0^\infty j_l(kr) g_{\kappa_2}(r) f_{\kappa_1}(r) dr, \quad (5)
\end{aligned}
$$

with the spherical Bessel function of the first kind j_l and the radial continuum wave functions g_κ and f_κ. The radial wave functions are obtained by solving the coupled radial Dirac equations

$$
\begin{aligned}
\frac{dg_\kappa}{dr} &= [E + 1 - V(r)] f_\kappa(r) - \frac{\kappa g_\kappa(r)}{r}, \\
\frac{df_\kappa}{dr} &= -[E - 1 - V(r)] g_\kappa(r) + \frac{\kappa f_\kappa(r)}{r}, \quad (6)
\end{aligned}
$$

where $V(r)$ is the electron-target interaction potential. In this work, pure Coulomb potential [$V(r) = -\frac{\alpha Z}{r}$, where α is the fine-structure constant] and Debye-Hückel (DH) screened potential [25,49] [$V(r) = -\frac{\alpha Z}{r} e^{-r/\delta}$, δ is the screening length in relativistic units] are investigated. To make the screening length more intuitive for different ions with effective Z, the scaled screening length can be defined as $D = \alpha \delta Z$ in atomic units. In addition, each radial integral of Eq. (5) is divided into two parts: the first part (0 to r_0) uses numerical quadrature

TABLE I. Comparison of the relativistic bremsstrahlung cross section for $Z = 13$ (Al^{13+}) and 79 (Au^{79+}) under pure Coulomb potential with Lee *et al.* [57].

| | | σ_k | | | |
| | | Al^{13+} | | Au^{79+} | |
T_1(keV)	k/T_1	Lee *et al.*	Present	Lee *et al.*	Present
	0.8	6.45	6.46	6.24	6.16
5	0.2	9.36	9.41	7.50	7.67
	0.8	4.56	4.51	6.78	6.70
50	0.2	9.08	9.09	9.30	9.32
	0.9	1.48	1.48	3.83	3.83
500	0.5	4.09	4.11	6.07	6.10

(as in [24]), and the second part (r_0 to ∞) uses analytical integrals, which are based on closed-form expressions of spherical Bessel functions. Details of calculating the radial wave function and overlap integral are given in the work by one of the coauthors [51].

To evaluate the angular distribution of bremsstrahlung cross sections, the normalized shape function is defined as the ratio of the differential cross section of photon energy and angle [$\sigma(k,\theta)$] to the photon energy spectrum [$\sigma(k)$] as [58,59]

$$S(\theta) = \frac{\sigma(k,\theta)}{\sigma(k)} = \frac{\sigma}{dkd\Omega_k} \bigg/ \frac{d\sigma}{dk}. \qquad (7)$$

The shape function depends on the atomic number Z or potential, initial electron kinetic energy T_1, and the fractional energy loss k/T_1.

III. RESULTS AND DISCUSSIONS

To verify the present calculations, Table I presents the relativistic bremsstrahlung cross sections for well-studied cases Al^{13+} and Au^{79+} compared with Lee *et al.* [57]. As it shows, the agreements between the values are quite good and the differences are basically around 0.1% for Al^{13+} and 1% for Au^{79+}, respectively. Investigations on the cross sections and angular distributions of bremsstrahlung of W^{74+} in a large energy range in pure Coulomb potential and Debye-Hückel screened potential are then reported. Note that in the present work, T_1 (T_2) and k are incident (outgoing) electron kinetic energy and emitted photon energy, respectively, and due to the conservation of energy, $T_1 = T_2 + k$.

Figure 1 presents the bremsstrahlung cross sections of W^{74+} in a pure Coulomb potential obtained by nonrelativistic dipole (NRD) and relativistic multipole (RM) calculations. It is evident that the cross sections obtained by both NRD and RM calculations tend to increase with increasing T_2 for a given T_1, and they decrease with increasing T_1 for a given T_2. In the present energy region, the NRD cross sections are smaller than the RM cross sections at relatively low incident energies (the cases of $T_1 \lesssim 50$ keV); while at relatively high incident energies (the cases of $T_1 \gtrsim 80$ keV), the bigger RM cross sections interchange with the NRD cross sections into smaller ones with the decreasing of T_2, and the intersection gradu-
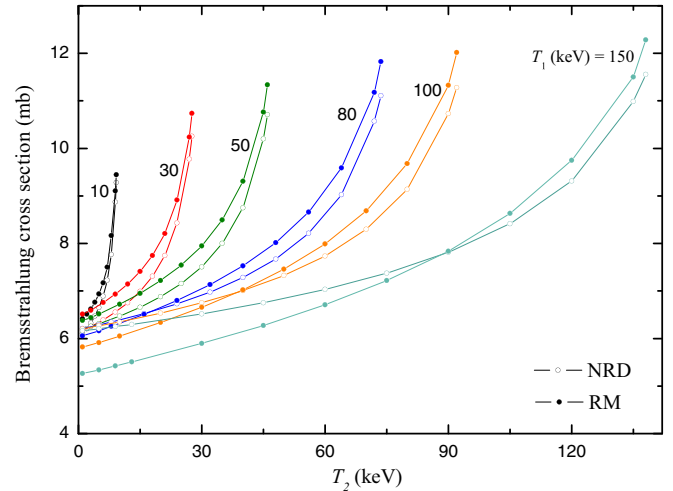

FIG. 1. Bremsstrahlung cross sections of W^{74+} in pure Coulomb potential by nonrelativistic dipole (NRD) and relativistic multipole (RM) calculations, and $T_1 = 10, 30, 50, 80, 100, 150$ keV.

ally shift towards higher T_2 as T_1 is increased from 80 keV to 150 keV.

The differences between NRD and RM cross sections are generally more significant at high incident energy (T_1), which is intuitively consistent with the importance of relativistic effect at high incident energies. For a fixed T_1, the relativistic effect indicated by the difference between NRD and RM cross sections decreases as T_2 is increased when $T_1 < 80$ keV, and it is more complicated at higher T_1. Those features demonstrate the interplay between the relativistic effects and the higher-order multipole effects because, in RM calculations, in addition to the relativistic wave functions for both initial and final states, the multipole expansion of the radiation field is also involved [60] (dipole approximation is employed in the NRD calculations). The photon multipole effect could be very important when emitting high-energy photons, corresponding to smaller T_2. The photon multipole effect seems to be more significant than the relativistic effect on the wave functions, they compete and contribute the RM cross sections together, resulting into the interchanges between NRD and RM cross sections. Actually, a similar cancellation between higher multipole and relativistic corrections to the NRD calculations has also been reported for low-Z elements [57,58]. For the bremsstrahlung of high-Z elements, the nonrelativistic dipole theory basically fails in the energy region of hundreds of keV, and relativistic multipole treatments are required to reveal the underlying physics and produce accurate cross sections in practical applications.

Given the fact that screened Coulomb interactions between charged particles appear and play a role in plasmas [40–48], the motions of electrons no longer take place in pure Coulomb potentials. For the typical weakly coupled classical plasmas as in magnetic confinement fusion with high temperature and low density [49], the well-known Debye-Hückel screened potential could be well employed for further investigations of the bremsstrahlung process. The RM bremsstrahlung cross sections of fully stripped tungsten (W^{74+}) in pure Coulomb and Debye-Hückel screened potentials with respect to T_2 for
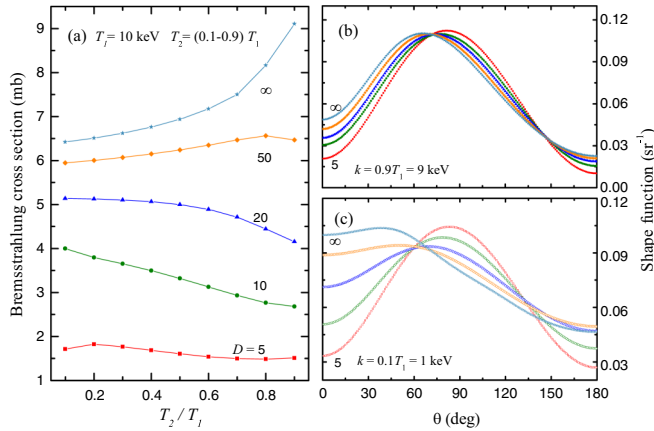
FIG. 2. The relativistic bremsstrahlung cross sections and its angular distributions of W^{74+} in pure Coulomb and Debye-Hückel potential $[V(r) = -\frac{\alpha Z}{r} e^{-r/\delta}$, δ is the screening length in relativistic units] at $T_1 = 10$ keV, and D(a.u.) $= \alpha\delta Z = 5, 10, 20, 50, \infty$ (pure Coulomb case).

FIG. 3. The angular distributions of relativistic bremsstrahlung of W^{74+} in pure Coulomb potential at $T_2 = 25$ keV, $k = 5$ keV.

$T_1 = 10$ keV are presented in Fig. 2(a). As it clearly shows, the plasmas' screening effect is very significant and important, the bremsstrahlung cross sections are suppressed and such a suppression becomes more and more significant as the screening length D is decreased (or the plasmas screening is increased) due to the reduction of interactions for the bremsstrahlung process. For example, the cross sections in pure Coulomb field is reduced by a factor of about 5 in plasmas for $D = 5$ a.u., and the suppression is more enhanced with respect to the increasing of outgoing electron energy T_2, it could be related to the different regions probed in the bremsstrahlung process and different multipole interactions for different T_2 [61].

The corresponding shape functions (angular distribution of bremsstrahlung cross sections) are presented in Figs. 2(b) and 2(c) at photon energy $k = 0.1T_1$ and $0.9T_1$, respectively. Dominant structures clearly exist in both shape functions, revealing that the emission of photons is more likely to happen around some specific angles. In the pure Coulomb potential, bremsstrahlung happens mainly at the small angles around 30° at $k = 0.1T_1$, while such an emission peak gradually shifts towards larger angles to about 60° at $k = 0.9T_1$. The preference of bremsstrahlung around some angles is consistent with the results revealed in Tseng's work [58]. Such features could be intuitively estimated from the principle of momentum conservation. A small value of k/T_1 implies a small momentum transfer and hence usually a small change of the direction of the electron during the elementary process of bremsstrahlung, whereas a small value of T_2/T_1 implies a large momentum transfer, and hence a greater possibility of large-angle scattering. These features can also be understood from a simpler physical image that the fast outgoing electron can not be easily altered and naturally prefers to fly along its incident direction, while both the outgoing electron and the emitted photon could be scattered away from its incident direction in the case of a slow outgoing electron. To conserve the total incident momentum, bremsstrahlung photons would be mainly emitted around the incident direction (small angles) in the case of the fast outgoing electron and low-energy emitted photon, while
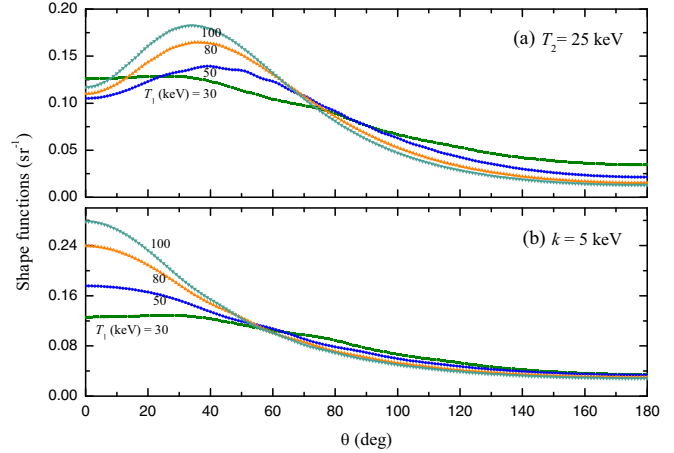
both the slow outgoing electron and emission photon would be more likely to be away from the incident direction (large angles) in the case with slow outgoing electron. If energies of both the incident and outgoing electrons are higher, their dynamics should be more difficult to be altered by the field, thus the shift of these peak structures to smaller angles.

As a further verification of these dynamics of peak structures, the shape functions with the incident electron energy of 30, 50, 80, and 100 keV in the pure Coulomb potential are shown in Fig. 3(a) with the same outgoing electron energy $T_2 = 25$ keV and in Fig. 3(b) with the same photon emission energy $k = 5$ keV, respectively. As it clearly shows, the photons are emitted mainly at the small angles, and the dominant structures generally move towards smaller angles as the energy of the incident electron is increased. These features are totally consistent with the above statements. Note that the results for low Z elements with respect to the increasing of photon energies by Tseng *et al.* have also verified these dynamics [58].

Another important feature in Figs. 2(b) and 2(c) is the variation of peak structure between the pure Coulomb potential and different screened potentials. In a screened potential, the effect of the field on the electron and the typical values of the distance between the nucleus and the interaction event (the "impact parameter") are all reduced. Switching on screening means weaker attraction between the electron and the nucleus, hence smaller impact parameters, thus lower cross sections, and this screening is more relevant the softer the emitted photon. For the emission of a photon with momentum kept fixed, smaller impact parameters are needed when screening is increased, therefore more large-angle bremsstrahlung emission could be predicted, just as shown in Fig. 2(c). The impact parameter is of the same order as the inverse minimum momentum transfer (in relativistic units) [61]. Thus, a decrease of the screening length causes an increase of the typical momentum transfers, and hence an increase of the probability of large-angle bremsstrahlung emission. Alternatively, in a screened potential, the continuum wave function around the nucleus for a given free energy would shift outwards, so that matrix element for the
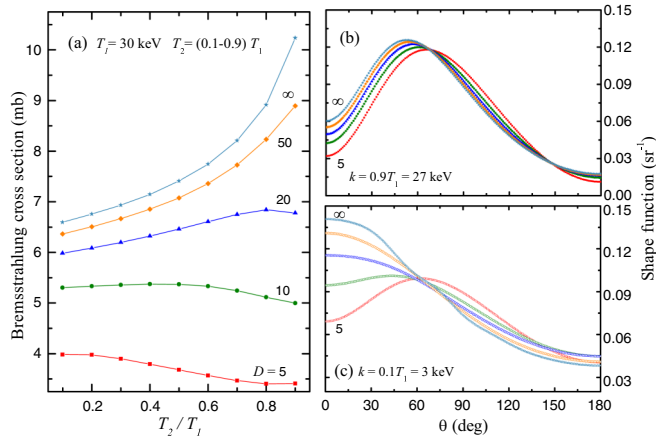
FIG. 4. Same as in Fig. 2, but $T_1 = 30$ keV.

bremsstrahlung process involves larger distance compared with that in pure Coulomb potential. Bearing in mind that the decrease of electron energies also results in an increase of the integration space of the matrix element, we would expect the cases with increasing the screening and decreasing the electron energies could produce similar bremsstrahlung results including peak variation dynamics. Accordingly, the peaks of the angular distributions shift towards larger angles when the screening length D is reduced. Consistently, Figs. 2(b) and 2(c) exactly reproduce the dynamics of emission peaks towards larger angles as the potential is softened from pure Coulomb to $D = 5$ a.u., causes a shift of the peaks to larger angles by about 25° and 45°, respectively. Note that for the bremsstrahlung in neutral atomic field, it can be also concluded that the screening effect increases as electron energy decreases [58].

The RM bremsstrahlung cross sections and the shape functions for $T_1 = 30$ keV and 150 keV are also presented to further verify the dynamics in screened field, shown in Figs. 4 and 5, respectively. It is evident that the main features are quite similar as the case of $T_1 = 10$ keV illustrated in Fig. 2, that the increasing screening effect significantly reduces the cross section and shifts the peak structure towards a larger angle; and the peak structure in the same pure Coulomb field or screened
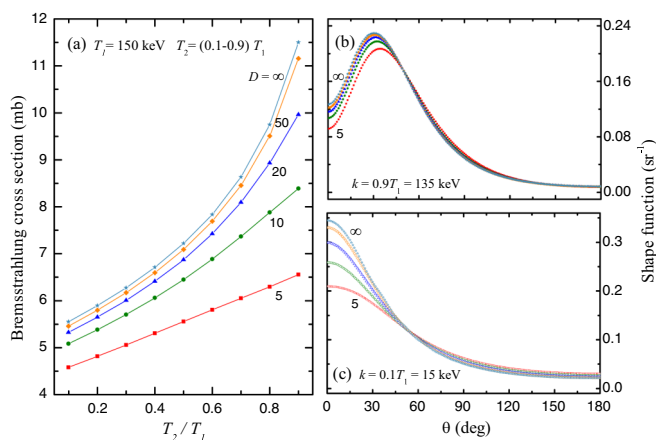
field also surely shift back to the incident energy direction as the energies of both incident and outgoing electron are increased (Figs. 2 to 5). As mentioned, all these features could be roughly estimated from the conservation of momentum and the decrease of typical impact parameters in a screened field. As T_1 is increased, the screening effect on the cross sections is reduced, and the peak structures locate more tightly in the small-angle region as in the case of a decrease of screening strength since the high-energy electrons are less affected by a change of screening.

IV. CONCLUSION

The bremsstrahlung cross sections of fully stripped tungsten (W^{74+}) and its angular distribution have been studied under pure Coulomb and Debye-Hückel potentials in a relativistic multipole framework. By comparing with nonrelativistic dipole results, it is concluded that for high Z elements, the nonrelativistic dipole theory basically fails in the energy region of hundreds of keV, and relativistic multipole treatments are essential for a reliable prediction of the cross sections. Furthermore, some important features are revealed from an in-depth study of the bremsstrahlung cross section and its angular distribution under different incident electron kinetic energies.

It is found that in the same potential field, as outgoing electron energy T_2 is increased, or the emitted photon energy k is increased, the scaled total bremsstrahlung cross sections corresponding to a given incident electron energy T_1 usually increase and a dominant structure, which is always exhibited at a small angle with respect to the incident electron direction, gradually shifts to smaller angles. Both the increase of cross section and the variation of the peak structure are mainly due to the conservation of momentum, leading to the increased probability that the photon will be emitted in roughly the same direction as the incident electron. The same features are also seen when T_1 is increased at a fixed T_2 or k. Some exceptions appear in Figs. 2 and 4 in cases of strong screening and low incident energies, when the cross sections do not change much or slightly decrease as T_2 increases. The increase of the screening effect suppresses the cross section from the pure Coulomb potential significantly at all incident electron energies, and this suppression is much more enhanced at high outgoing electron energy T_2 and lower incident electron energy T_1. Furthermore, the increase of the screening effect would also suppress the dominant behavior of cross sections at small angles and shift the peak structure to a larger angle. These features could be explained by the fact that a stronger screening causes a reduction of the maximum value of impact parameter and hence an increase of the minimum relative momentum transfer. This increase, in turn, implies an increased probability of large-angle bremsstrahlung emission. This is similar to the case of a slow outgoing electron because a large reduction of the electron energy during the elementary process of bremsstrahlung is also accompanied by a relatively large momentum transfer.

In summary, the main features of the bremsstrahlung cross sections of W^{74+} are reported and the physics behind it are fully discussed, which should be helpful in a deep understanding of the bremsstrahlung process and the screening effects

FIG. 5. Same as in Fig. 2, but $T_1 = 150$ keV.

in plasmas. The present relativistic treatment for the plasma screening effect and numerical procedure of obtaining the cross sections are validated in the present work. The extension to other ions in the future is straightforward, where a distorted potential would be adopted to include the screening effect from atomic electrons.

[1] M. Firdaouss, C. Desgranges, C. Hernandez, C. Mateus, H. Maier, B. Böswirth, H. Greuner, F. Samaille, J. Bucalossi, and M. Missirlian, Tungsten coating by ATC plasma spraying on CFC for WEST tokamak, Phys. Scr. **2017**, 014008 (2017).

[2] L. Begrambekov, A. Gordeev, Y. Ma, G. Vayakis, P. Shigin, Y. Sadovsky, A. Zakharov, and M. Walsh, Development of quality tungsten coating on ceramics as a microwave shield for ITERHigh-frequency Magnetic Sensor, Fusion Sci. Technol. **76**, 1 (2020).

[3] D. Wu, L. Zhang, P. Liu, L. Sun, R. Hai, and H. Ding, Diagnostic study of laser-produced tungsten plasma using optical emission spectroscopy and time-of-flight mass spectroscopy, Spectrochim. Acta. B **137**, 70 (2017).

[4] A. V. Gurevich, On the theory of runaway electrons, Sov. Phys. JETP **12**, 904 (1961).

[5] R. M. Kulsrud, Y.-C. Sun, N. K. Winsor, and H. A. Fallon, Runaway Electrons in a Plasma, Phys. Rev. Lett. **31**, 690 (1973).

[6] J. W. Connor and R. J. Hastie, Relativistic limitations on runaway electrons, Nucl. Fusion **15**, 415 (1975).

[7] D. Hwangbo, S. Kawaguchi, S. Kajita, and N. Ohno, Erosion of nanostructured tungsten by laser ablation, sputtering and arcing, Nucl. Mater. Energy **12**, 386 (2017).

[8] C. Guillemaut, A. Jardin, J. Horacek, I. Borodkina, A. Autricque, G. Arnoux, J. Boom, S. Brezinsek, J. Coenen, and E. De La Luna, Experimental estimation of tungsten impurity sputtering due to Type IELMs in JET-ITER-like wall using pedestal electron cyclotron emission and target Langmuir probe measurements, Phys. Scr. **2016**, 014005 (2016).

[9] D. E. Post and R. Behrisch, *Physics of Plasma-Wall Interactions in Controlled Fusion* (Springer Science & Business Media, New York, 2013).

[10] V. Philipps, Plasma-wall interaction, a key issue on the way to a steady state burning fusion device, Phys. Scr. **2006**, 24 (2006).

[11] A. Kirschner, V. Philipps, J. Winter, and U. Kögler, Simulation of the plasma-wall interaction in a tokamak with the Monte Carlo code ERO − TEXTOR, Nucl. Fusion **40**, 989 (2000).

[12] F. C. Schuller, Disruptions in tokamaks, Plasma Phys. Contr. F. **37**, A135 (1995).

[13] A. H. Boozer, Theory of tokamak disruptions, Phys. Plasmas **19**, 058101 (2012).

[14] G. Jahns, M. Soler, B. Waddell, J. Callen, and H. Hicks, Internal disruptions in tokamaks, Nucl. Fusion **18**, 609 (1978).

[15] D. Post, A review of recent developments in atomic processes for divertors and edge plasmas, J. Nucl. Mater. **220-222**, 143 (1995).

[16] W. M. Stacey, *Fusion: An Introduction to the Physics and Technology of Magnetic Confinement Fusion* (John Wiley & Sons, New York, 2010).

[17] G. B. Rybicki and A. P. Lightman, *Radiative Processes in Astrophysics* (John Wiley & Sons, New York, 2008).

[18] N. B. Delone, *Basics of Interaction of Laser Radiation with Matter* (Atlantica Sèguier Frontières, Paris, 1993).

[19] R. Parker, G. Janeschitz, H. D. Pacher, D. Post, S. Chiocchio, G. Federici, P. Ladd, and I. J. C. Teama, Plasma-wall interactions in ITER, J. Nucl. Mater. **241-243**, 1 (1997).

[20] R. W. Conn and J. Kesner, Plasma modeling and first wall interaction phenomena in tokamaks, J. Nucl. Mater. **63**, 1 (1976).

[21] R. V. Jensen, D. Post, W. Grasberger, C. Tarter, and W. Lokke, Calculations of impurity radiation and its effects on tokamak experiments, Nucl. Fusion **17**, 1187 (1977).

[22] V. Vershkov and S. Mirnov, Role of impurities in current tokamak experiments, Nucl. Fusion **14**, 383 (1974).

[23] D. K. Morozov, E. Baronova, and I. Y. Senichenkov, Impurity radiation from a tokamak plasma, Plasma Phys. Rep. **33**, 906 (2007).

[24] H. K. Tseng and R. H. Pratt, Exact screened calculations of atomic-field bremsstrahlung, Phys. Rev. A **3**, 100 (1971).

[25] J. Y. Wu, Y. Wu, Y. Y. Qi, J. G. Wang, R. K. Janev, and S. B. Zhang, Resonances in nonrelativistic free-free Gaunt factors with screened Coulomb interaction, Phys. Rev. A **99**, 012705 (2019).

[26] H. Bethe and W. Heitler, On the stopping of fast particles and on the creation of positive electrons, Proc. R. Soc. Lond. Ser. A **146**, 83 (1934).

[27] G. Elwert, Verschärfte berechnung von intensität und polarisation im kontinuierlichen räntgenspektrum1, Ann. Phys. (Leipzig) **426**, 178 (1939).

[28] G. Elwert and E. Haug, Calculation of bremsstrahlung cross sections with Sommerfeld-Maue eigenfunctions, Phys. Rev. **183**, 90 (1969).

[29] R. Pratt, H. Tseng, C. Lee, L. Kissel, C. MacCallum, and M. Riley, Bremsstrahlung energy spectra from electrons of kinetic energy $1 \text{ keV} \leqslant T_1 \leqslant 2000 \text{ keV}$ incident on neutral atoms $2 \leqslant Z \leqslant 92$, At. Data Nucl. Data Tables **20**, 175 (1977).

[30] L. Kissel, C. MacCallum, and R. Pratt, Bremsstrahlung energy spectra from electrons of kinetic energy 1 keV less than or equal to T less than or equal to 2000 keV incident on neutral atoms 1 less than or equal to Z less than or equal to 92, At. Data Nucl. Data Tables **26**, 477 (1981).

[31] V. A. Yerokhin and A. Surzhykov, Electron-atom bremsstrahlung: Double-differential cross section and polarization correlations, Phys. Rev. A **82**, 062702 (2010).

[32] O. Kovtun, V. Tioukine, A. Surzhykov, V. A. Yerokhin, B. Cederwall, and S. Tashenov, Spin-orbit interaction in bremsstrahlung and its effect on the electron motion in a strong Coulomb field, Phys. Rev. A **92**, 062707 (2015).

[33] D. H. Jakubassa-Amundsen, Electron–heavy-nucleus bremsstrahlung at highly relativistic impact energies, Phys. Rev. A **82**, 042714 (2010).

[34] D. H. Jakubassa-Amundsen, Relativistic theory for the elementary process of bremsstrahlung induced by heavy spin-zero nuclei, Phys. Rev. A **93**, 052716 (2016).

[35] S. M. Seltzer, An overview of ETRAN Monte Carlo methods, in *Monte Carlo Transport of Electrons and Photons* (Springer, New York, 1988), pp. 153–181.

[36] A. F. Bielajew, R. Mohan, and C.-S. Chui, Improved bremsstrahlung photon angular sampling in the EGS4 code system, National Research Council of Canada Report PIRS-0203 (1989).

[37] L. Pandola, C. Andenna, and B. Caccia, Validation of the Geant4 simulation of bremsstrahlung from thick targets below 3 Mev, Nucl. Instrum. Meth. B **350**, 41 (2015).

[38] Y. Y. Qi, J. G. Wang, and R. K. Janev, Bound-bound transitions in hydrogenlike ions in Debye plasmas, Phys. Rev. A **78**, 062511 (2008).

[39] Y. Y. Qi, J. G. Wang, and R. K. Janev, Dynamics of photoionization of hydrogenlike ions in Debye plasmas, Phys. Rev. A **80**, 063404 (2009).

[40] S. B. Zhang, J. G. Wang, R. K. Janev, and X. J. Chen, Electron-hydrogen atom-impact $1s \rightarrow 2s$ and $1s \rightarrow 2p$ excitation with screened Coulomb interaction between the $n = 2$ and $n = 3$ excitation thresholds, Phys. Rev. A **83**, 032724 (2011).

[41] S. B. Zhang, J. G. Wang, and R. K. Janev, Crossover of Feshbach Resonances to Shape-Type Resonances in Electron-Hydrogen Atom Excitation with a Screened Coulomb Interaction, Phys. Rev. Lett. **104**, 023203 (2010).

[42] S. B. Zhang, J. G. Wang, and R. K. Janev, Electron-hydrogen-atom elastic and inelastic scattering with screened Coulomb interaction around the $n = 2$ excitation threshold, Phys. Rev. A **81**, 032707 (2010).

[43] S. B. Zhang, J. G. Wang, R. K. Janev, Y. Z. Qu, and X. J. Chen, Photodetachment of hydrogen negative ions with screened Coulomb interaction, Phys. Rev. A **81**, 065402 (2010).

[44] R. K. Janev, S. B. Zhang, and J. G. Wang, Review of quantum collision dynamics in Debye plasmas, Matter Radiat. Extrem. **1**, 237 (2016).

[45] E. Braaten and T. C. Yuan, Calculation of Screening in a Hot Plasma, Phys. Rev. Lett. **66**, 2183 (1991).

[46] L. G. Stanton and M. S. Murillo, Unified description of linear screening in dense plasmas, Phys. Rev. E **91**, 033104 (2015).

[47] C. Y. Lin and Y. K. Ho, Effects of screened Coulomb (yukawa) and exponential-cosine-screened Coulomb potentials on photoionization of H and He$^+$, Eur. Phys. J. D **57**, 21 (2010).

[48] J. Li, S. B. Zhang, B. J. Ye, J. G. Wang, and R. K. Janev, Low-energy electron elastic scattering and impact ionization with hydrogenlike helium in debye plasmas, Phys. Rev. A **96**, 032707 (2017).

[49] J. Y. Wu, Y. Y. Qi, Y. J. Cheng, Y. Wu, J. G. Wang, R. K. Janev, and S. B. Zhang, Free-free gaunt factors of hydrogen-like ions in dense quantum plasmas, Phys. Plasmas **27**, 043301 (2020).

[50] J. Y. Wu, Y. Wu, Y. Y. Qi, J. G. Wang, R. Janev, and S. B. Zhang, Non-relativistic free-free gaunt factors in Debye plasmas, Mon. Not. R. Astron. Soc. **486**, 141 (2019).

[51] A. Poškus, BREMS: A program for calculating spectra and angular distributions of bremsstrahlung at electron energies less than 3 Mev, Comput. Phys. Commun. **232**, 237 (2018).

[52] R. H. Pratt, A. Ron, and H. K. Tseng, Atomic photoelectric effect above 10 keV, Rev. Mod. phys. **45**, 273 (1973).

[53] H. W. Koch and J. W. Motz, Bremsstrahlung cross-section formulas and related data, Rev. Mod. Phys. **31**, 920 (1959).

[54] J. A. García-Alvarez, J. M. Fernàndez-Varea, V. R. Vanin, and N. L. Maidana, Electron-atom bremsstrahlung cross sections in the 20-100 keV energy region: Absolute measurements for and comparison with theoretical databases, J. Phys. B: At. Mol. Opt. Phys. **51**, 225003 (2018).

[55] A. V. Korol, O. I. Obolensky, A. V. Solov'yov, and I. A. Solovjev, The full relativistic description of the bremsstrahlung process in a charged particle-atom collision, J. Phys. B: At. Mol. Opt. Phys. **34**, 1589 (2001).

[56] W. J. Karzas and R. Latter, Electron radiative transitions in a coulomb field, Astrophys. J. Suppl. S. **6**, 167 (1961).

[57] C. M. Lee, L. Kissel, R. H. Pratt, and H. K. Tseng, Electron bremsstrahlung spectrum, 1–500 keV, Phys. Rev. A **13**, 1714 (1976).

[58] H. K. Tseng, R. H. Pratt, and C. M. Lee, Electron bremsstrahlung angular distributions in the 1–500 keV energy range, Phys. Rev. A **19**, 187 (1979).

[59] L. Kissel, C. A. Quarles, and R. H. Pratt, Shape functions for atomic-field bremsstrahlung from electrons of kinetic energy 1-500 keV on selected neutral atoms $1 \leqslant Z \leqslant 92$, Atom. Data Nucl. Data **28**, 381 (1983).

[60] M. S. Wang, Y. S. Kim, R. H. Pratt, and A. Ron, Observation of zeros and amplification of quadrupole-matrix-element contributions to photoelectron angular distributions, Phys. Rev. A **25**, 857 (1982).

[61] R. H. Pratt and I. J. Feng, in *Electron-Atom Bremsstrahlung*, Atomic Inner-Shell Physics (Springer, New York, 1985), pp. 533–580.